PROBING THE INTERSTELLAR MEDIUM AND STAR FORMATION OF THE MOST LUMINOUS QUASAR AT z = 6.3

CrossMark

PROBING THE INTERSTELLAR MEDIUM AND STAR FORMATION OF THE MOST LUMINOUS QUASAR AT $z = 6.3$

Ran Wang[1], Xue-Bing Wu[1,2], Roberto Neri[3], Xiaohui Fan[1,4], Fabian Walter[5], Chris L. Carilli[6], Emmanuel Momjian[6], Frank Bertoldi[7], Michael A. Strauss[8], Qiong Li[2], Feige Wang[2], Dominik A. Riechers[9], Linhua Jiang[1], Alain Omont[10], Jeff Wagg[11], and Pierre Cox[12]

[1] Kavli Institute of Astronomy and Astrophysics at Peking University, No. 5 Yiheyuan Road, Haidian District, Beijing, 100871, China
[2] Department of Astronomy, School of Physics, Peking University, No. 5 Yiheyuan Road, Haidian District, Beijing, 100871, China
[3] Institute de Radioastronomie Millimetrique, St. Martin d'Heres, F-38406, France
[4] Steward Observatory, University of Arizona, 933 N. Cherry Avenue, Tucson, AZ 85721, USA
[5] Max-Planck-Institute for Astronomy, Königsstuhl 17, D-69117 Heidelberg, Germany
[6] National Radio Astronomy Observatory, P.O. Box 0, Socorro, NM 87801, USA
[7] Argelander-Institut für Astronomie, University of Bonn, Auf dem Hügel 71, D-53121 Bonn, Germany
[8] Department of Astrophysical Sciences, Princeton University, Princeton, NJ 08544, USA
[9] Astronomy Department, Cornell University, 220 Space Sciences Building, Ithaca, NY 14853, USA
[10] Institut d'Astrophysique de Paris, UMR 7095, CNRS and Universite Pierre et Marie Curie, Paris, France
[11] Square Kilometre Array Organisation, Jodrell Bank Observatory, Jodrell Bank, Macclesfield SK11 9DL, UK
[12] Joint ALMA Observatory, Alonso de Córdova 3107, Vitacura, Santiago, Chile

ABSTRACT

We report new IRAM/PdBI, JCMT/SCUBA-2, and VLA observations of the ultraluminous quasar SDSS J010013.02+280225.8 (hereafter, J0100+2802) at $z = 6.3$, which hosts the most massive supermassive black hole (SMBH), $1.24 \times 10^{10} M_\odot$, that is known at $z > 6$. We detect the [C II] 158 μm fine structure line and molecular CO(6-5) line and continuum emission at 353, 260, and 3 GHz from this quasar. The CO(2-1) line and the underlying continuum at 32 GHz are also marginally detected. The [C II] and CO detections suggest active star formation and highly excited molecular gas in the quasar host galaxy. The redshift determined with the [C II] and CO lines shows a velocity offset of $\sim$1000 km s^{-1} from that measured with the quasar Mg II line. The CO (2-1) line luminosity provides a direct constraint on the molecular gas mass, which is about $(1.0 \pm 0.3) \times 10^{10} M_\odot$. We estimate the FIR luminosity to be $(3.5 \pm 0.7) \times 10^{12} L_\odot$, and the UV-to-FIR spectral energy distribution of J0100 +2802 is consistent with the templates of the local optically luminous quasars. The derived [C II]-to-FIR luminosity ratio of J0100+2802 is 0.0010 ± 0.0002, which is slightly higher than the values of the most FIR luminous quasars at $z \sim 6$. We investigate the constraint on the host galaxy dynamical mass of J0100+2802 based on the [C II] line spectrum. It is likely that this ultraluminous quasar lies above the local SMBH–galaxy mass relationship, unless we are viewing the system at a small inclination angle.

Key words: galaxies: evolution – galaxies: high-redshift – galaxies: starburst – quasars: individual (SDSS J010013.02+280225.8)

1. INTRODUCTION

An ultraluminous quasar, SDSS J010013.02+280225.8 (hereafter, J0100+2802), with a bolometric luminosity of $L_{\rm bol} = 4.3 \times 10^{14} L_\odot$ and a supermassive black hole (SMBH) mass of $M_{\rm BH} \approx 1.2 \times 10^{10} M_\odot$, was discovered at $z = 6.3$ (Wu et al. 2015). This is by far the most optically luminous object, with the most massive SMBH among the $\sim$50 quasars known at $z > 6$ (Fan et al. 2006; Willott et al. 2010; Bañados et al. 2014; Jiang et al. 2015; Venemans et al. 2015; Matsuoka et al. 2016), and the SMBH mass is also comparable to the highest value found in the local universe (McConnell et al. 2011; Thomas 2016). It demonstrates that such a rare, $10^{10} M_\odot$ SMBH, could be formed as early as $z \gtrsim 6.3$, when the age of the universe was only 890 Myr.

Recent submillimeter and millimeter [(sub)mm] surveys detected strong far-infrared (FIR) continuum, molecular CO, and [C II] 158 μm fine structure line emission in the host galaxies of a number of quasars at $z > 5.7$ (e.g., Bertoldi et al. 2003; Priddey et al. 2003; Robson et al. 2004; Walter et al. 2004; Carilli et al. 2007; Wang et al. 2010, 2013; Omont et al. 2013; Willott et al. 2015; Venemans et al. 2016). The results argue for significant host galaxy evolution with active

star formation in these young quasars in the early universe, and the [C II] line images at sub-second resolution constrain the radius of the nuclear starburst region to be a few kiloparsecs (Leipski et al. 2013; Wang et al. 2013; Venemans et al. 2016). The gas dynamics measured with the CO and [C II] observations suggest SMBH-host mass ratios of a factor of a few to one order of magnitude higher than the present-day value (Walter et al. 2004; Wang et al. 2013; Willott et al. 2015; Venemans et al. 2016).

The most massive $z > 6$ quasar-galaxy systems studied in previous millimeter and radio observations are objects with SMBH masses of a few $10^9 M_\odot$ and $L_{\rm bol} \lesssim 10^{14} L_\odot$ (e.g., Wang et al. 2013; Willott et al. 2015; Venemans et al. 2016). The discovery of J0100+2802 provides a unique chance to study the quasar-galaxy co-evolution in the system that hosts the most massive known SMBH at the earliest epoch. In this work, we report our new observations of the (sub)mm and radio continuum, [C II] 158 μm, and molecular CO lines from the host galaxy of J0100+2802. The observations are described in Section 2, and the results are presented in Section 3. We discuss the quasar spectral energy distribution (SED), FIR continuum, [C II], and CO line ratios, and the constraints of the host galaxy dynamical mass in Section 4, and summarize the

results in Section 5. A Λ-CDM cosmology with $H_0 = 71$ km s^{-1} Mpc^{-1}, $\Omega_M = 0.27$, and $\Omega_\Lambda = 0.73$ is adopted throughout this paper (Spergel et al. 2007).

2. OBSERVATIONS

2.1. Plateau de Bure Interferometer (PdBI) Observations

We observed the [C II] 158 μm ($^2P_{3/2}$–$^2P_{1/2}$) and molecular CO(6-5) line emission from J0100+2802 using the PdBI. The observations were carried out during summer 2014 in the D-configuration using five antennas. We used the WideX wideband correlator in dual polarization with a total bandwidth of 3.6 GHz. We setup the correlator centered at the frequency of 260.35 GHz for the [C II] line and 94.72 GHz for the CO(6-5) line. This corresponds to the quasar Mg II line redshift of $z = 6.30$ (Wu et al. 2015). The flux density scale was determined based on observations of the standard flux density calibrator MWC349, and the typical calibration uncertainties are 10% at 3 mm and 20% at 1 mm. The phase was checked about every 22 minutes by observing a nearby phase calibrator, J0112+321. We reduced the data using the Grenoble Image and Line Data Analysis System (GILDAS) software (Guilloteau & Lucas 2000). The maps were made using natural weighting. The FWHM synthesized beam sizes are 2″00 × 1″66 and 5″41 × 4″31 at the [C II] and CO(6-5) frequencies, respectively. The final rms sensitivity of the [C II] line observation is 2.3 mJy beam^{-1} per 46 km s^{-1} channel, with a total on-source integration time of 4.5 hr, and the rms of the CO(6-5) observation is 0.42 mJy beam^{-1} per 63 km s^{-1} channel in 13.2 hr.

2.2. VLA Observations

We observed the CO(2-1) line emission with the Karl G. Jansky Very Large Array (VLA) in the *Ka*-Band ($\sim$32 GHz) in C-configuration during 2014 October–November, and the 3 GHz radio continuum in the *S*-band in A-configuration during 2015 June. The observations were performed using the WIDAR correlator with the 8-bit sampler in dual polarization. The setup covers a total bandwidth of 2 GHz, with 16 128 MHz spectral windows and the channel width in each spectral window is 2 MHz. We have spent a total on-source observing time of 7.2 hr for the CO(2-1) line observation and 2.1 hr for the 3 GHz continuum. The flux density calibration was carried out using the standard VLA calibrator 3C48, with typical calibration uncertainties better than 5%. The phases were checked with nearby point sources.

We reduced the data using the Common Astronomy Software Applications package (CASA v4.4) and the VLA calibration pipeline version 1.3.4. The FWHM synthesized beam size is 0″74 × 0″68 at 32 GHz and 0″65 × 0″54 at 3 GHz, using robust weighting. For the CO(2-1) line observations, we binned the data to a channel width of 57 km s^{-1}, and obtained a typical 1σ rms noise of 0.067 mJy beam^{-1} per channel. The channels affected by radio frequency interference were removed in the *S*-Band observations, resulting in a useful frequency range of $\sim$2.4 to 4 GHz and a bandwidth of about 1.6 GHz. The final continuum sensitivity at 3 GHz was 3.1 μJy beam^{-1}.

Table 1
Line and Continuum Properties of J0100+2802

[C II] redshift	6.3258 ± 0.0010
[C II] FWHM (km s^{-1})	300 ± 77
[C II] line flux (Jy km s^{-1})	3.36 ± 0.46
[C II] line luminosity:	
($L_\odot$)	$(3.56 \pm 0.49) \times 10^9$
(K km s^{-1} pc^2)	$(1.62 \pm 0.22) \times 10^{10}$
CO(6-5) redshift	6.3264 ± 0.0024
CO(6-5) FWHM (km s^{-1})	498 ± 225
CO(6-5) line flux (Jy km s^{-1})	0.32 ± 0.084
CO(6-5) line luminosity:	
($L_\odot$)	$(1.23 \pm 0.32) \times 10^8$
(K km s^{-1} pc^2)	$(1.17 \pm 0.30) \times 10^{10}$
CO(2-1) line flux (Jy km s^{-1})	0.038 ± 0.013
CO(2-1) line luminosity:	
($L_\odot$)	$(4.89 \pm 1.67) \times 10^6$
(K km s^{-1} pc^2)	$(1.25 \pm 0.43) \times 10^{10}$
CO(1-0) line luminosity (derived from the CO (2-1) line):	
($L_\odot$)	$(6.11 \pm 2.09) \times 10^5$
(K km s^{-1} pc^2)	$(1.25 \pm 0.43) \times 10^{10}$
666 GHz continuum (mJy)	<30
353 GHz continuum (mJy)	4.1 ± 1.2
260 GHz continuum (mJy)	1.35 ± 0.25
94.5 GHz continuum (mJy)	<0.1
32 GHz continuum (μJy)	14.8 ± 4.3
3 GHz continuum (μJy)	104.5 ± 3.1
FIR luminosity ($L_\odot$):	
$T_{dust} = 47$ K, $\beta = 1.6$	$(3.5 \pm 0.7) \times 10^{12}$
$T_{dust} = 40$ K, $\beta = 1.6$	$(2.4 \pm 0.5) \times 10^{12}$
$T_{dust} = 60$ K, $\beta = 1.6$	$(6.0 \pm 1.2) \times 10^{12}$
dust mass ($M_\odot$):	
$T_{dust} = 47$ K, $\beta = 1.6$	$(2.0 \pm 0.4) \times 10^8$
$T_{dust} = 40$ K, $\beta = 1.6$	$(3.1 \pm 0.6) \times 10^8$
$T_{dust} = 60$ K, $\beta = 1.6$	$(1.1 \pm 0.2) \times 10^8$

2.3. SCUBA-2 Observations

We observed the 450 μm (666 GHz) and 850 μm (353 GHz) dust continuum from J0100+2802 using the Submillimetre Common-User Bolometer Array 2 (SCUBA-2; Holland et al. 2013) on the James Clerk Maxwell Telescope (JCMT) during 2015 November. The observations were carried out in Band 2 weather conditions (i.e., $0.05 < \tau_{225\,GHz} < 0.008$), and in "CV DAISY" mode, which is designed for point/compact source observations. The beam size of SCUBA-2 is 7″9 at 666 GHz and 13″ at 353 GHz. We observed the target in four 30 minute scans with a total on-source time of $\sim$2 hr. The data was reduced using the STARLINK SCUBA-2 pipeline for faint point sources (Chapin et al. 2013), and we obtained a 1σ point-source sensitivity of 1.2 mJy at 353 GHz and 10 mJy at 666 GHz.

3. RESULTS

We summarize the measurements of redshift, line flux, FWHM line width, and luminosity of the [C II], CO(6-5), and CO(2-1) lines, as well as the continuum in Table 1. The [C II] and CO(6-5) lines are clearly detected (Figure 1), as well as the continuum emission at 353, 260, and 3 GHz. We fit a Gaussian line profile to the [C II] and CO(6-5) line spectra to determine the redshifts and line widths, and integrate the continuum-subtracted data over the line-emitting channels to get the line flux. The redshifts and line widths measured on the [C II] and
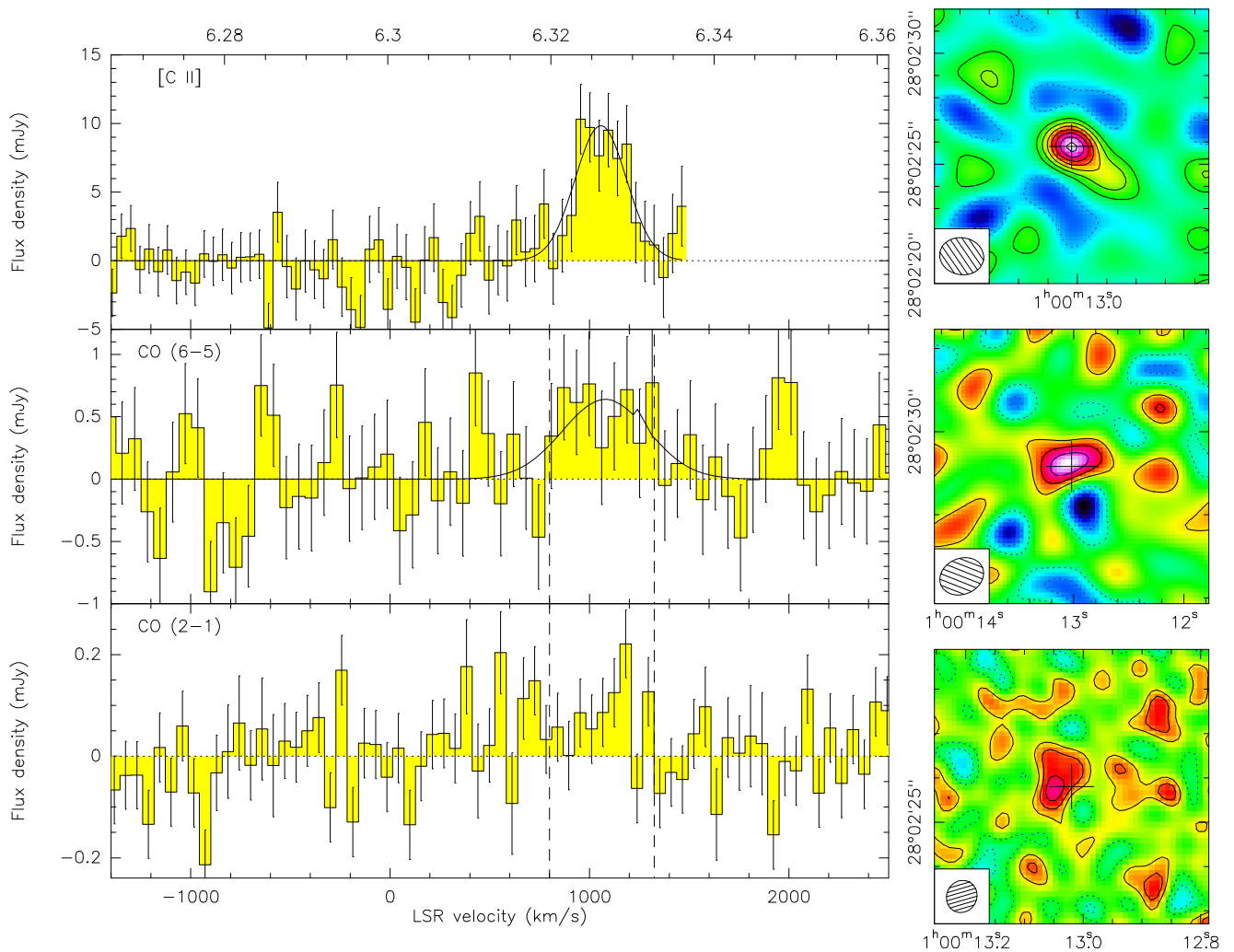
Figure 1. Line spectra (left) and velocity-integrated map (right) of the [C II] 158 μm (upper panel), CO(6-5) (middle panel), and CO(2-1) line emission (lower panel) from J0100+2802. The bottom abscissa shows the radio velocity in Kinematic Local Standard of Rest (LSRK) frame, where zero velocity corresponds to $z_{Mg\,II} = 6.30$ (Wu et al. 2015). The top abscissa denotes the corresponding redshift. The contours for the [C II] line intensity map are $[-2, -1, 1, 2, 3, 4, 5, 6, 7] \times 0.77$ mJy beam^{-1}, and $[-2, -1, 1, 2, 3] \times 0.15$ mJy beam^{-1} for the CO (6-5) line. The CO(2-1) line intensity map is obtained by integrating over the velocity range defined by the CO(6-5) line (vertical dashed lines), and contours are $[-2, -1, 1, 2, 3] \times 23$ μJy beam^{-1}. The cross in each panel denotes the position of the optical quasar, and the synthesized beams are plotted at the bottom left of each map.

CO(6-5) lines are consistent with each other within the errors, and we adopt $z_{[C\,II]} = 6.3258 \pm 0.0010$ as the redshift of the quasar host galaxy. We obtain tentative detections for the CO(2-1) line and the 32 GHz continuum. The central frequency and width of the CO(2-1) line are difficult to constrain due to the poor signal-to-noise ratio (S/N) of the spectrum. We integrate the visibility data over the velocity range of the CO(6-5) line emission (i.e., 800 km s^{-1} to 1300 km s^{-1} in Figure 1), and the intensity map shows a 3.6σ peak about 0″.27 away from the optical quasar position. Considering the measurement uncertainties and the astrometric mismatch between the radio and optical frames, this is consistent with the quasar optical position. We also measure the 32 GHz continuum emission to be $S_{32\,GHz} = 14.8 \pm 4.3$ μJy by averaging all the line-free spectral windows. We subtract the continuum from the line-emitting channels, resulting in a CO(2-1) line flux of 0.038 ± 0.013 Jy km s^{-1} at the peak position. Due to the poor S/N of the intensity map, we cannot obtain reliable measurement of the source size or address if there are more extended components with lower surface brightness.

The quasar Mg II line emission from J0100+2802 measures a redshift of $z_{Mg\,II} = 6.301 \pm 0.006$ (Figure 3 in Wu et al. 2015), which is blueshifted by 1020 ± 250 km s^{-1} compared to $z_{[C\,II]}$. Similar blueshifted Mg II lines with velocity offsets of a few hundred to 1700 km s^{-1} are also detected in several other $z > 6$ quasars (Willott et al. 2015; Venemans et al. 2016). Such large Mg II line velocity offsets with respect to the quasar host galaxy redshift are rare at low redshift (Richards et al. 2002), and may suggest outflowing gas in the broad line region at an early evolutionary phase. A larger sample of high-z quasars with $z_{Mg\,II}$ and $z_{[C\,II]}$ measurements is required to investigate the relationship between Mg II velocity offset and quasar luminosities (Venemans et al. 2016) and address the origin of the blueshifted quasar Mg II line.

4. DISCUSSION

4.1. Continuum Emission and SED

The new observations we present here measure the rest-frame FIR to radio continuum emission from J0100+2802. We
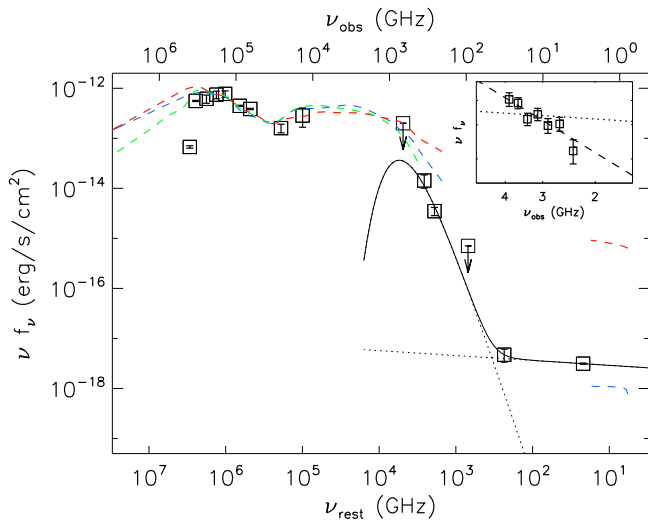
Figure 2. Rest-frame UV-to-radio SED of J0100+2802. The squares show the data from SDSS, 2MASS, and *WISE* (Wu et al. 2015), and the new measurements in this work. The arrows denote 3σ upper limits. The templates of local radio-quiet (blue line) and radio-loud quasars (red line, Elvis et al. 1994) and SDSS optically luminous quasars (green line, Richards et al. 2006) are plotted and scaled to the 2MASS *H*-band flux. The dotted lines are the graybody and power-law (with $f_\nu \sim \nu^\alpha$ and $\alpha_{22\,\mathrm{GHz}}^{234\,\mathrm{GHz}} = -0.90$) fit to the FIR and radio continuum, respectively, and the black solid line shows the total emission from these two components. The inner panel shows the *S*-band continuum fluxes measured in every 258 MHz frequency bins from 2.3 to 4 GHz. The dotted line is the power law with $\alpha_{22\,\mathrm{GHz}}^{234\,\mathrm{GHz}} = -0.90$ fitted to the *Ka*-band continuum and the *S*-band flux density averaged over the total 1.6 GHz bandwidth, while the dashed line is the best-fitting result to only the *S*-band data with $\alpha_{22\,\mathrm{GHz}} = -0.06$.

plot the SED of J0100+2802 in Figure 2 (Wu et al. 2015), together with the data from SDSS, the Two Micron All Sky Survey (2MASS), and the *Wide-field Infrared Survey Explorer* (*WISE*). The templates of optically luminous quasars from Elvis et al. (1994) and Richards et al. (2006) are also plotted for comparison. We scale the templates to the 2MASS *H*-band flux, and the (sub)mm measurements show no excess compared to the FIR emission of the scaled templates. We cannot rule out that the FIR continuum emission from J0100+2802 is dominated by thermal emission from the active galactic nucleus (AGN)-heated dust. However, the detections of [C II] and CO line emission do argue for a star-forming interstellar medium (ISM) in the nuclear region (see Section 4.2). We fit the (sub)mm flux densities to an optically thin graybody model with a dust temperature of $T_{\mathrm{dust}} = 47$ K and an emissivity index of $\beta = 1.6$ from the (sub)mm-detected quasars at $z > 1.7$ (Beelen et al. 2006). This results in a FIR (42.5–122.5 μm) luminosity of $L_{\mathrm{FIR}} = (3.5 \pm 0.7) \times 10^{12}\,L_\odot$, and a 8–1000 μm IR luminosity of $L_{\mathrm{IR}} = (5.0 \pm 0.9) \times 10^{12}\,L_\odot$. The star formation rate (SFR) estimated with the IR luminosity using the relation in Kennicutt (1998) is 850 $M_\odot$ yr^{-1}. As the fraction contributed from the torus is unknown, this constrains the upper limits of the star formation-powered FIR emission and SFR in the host galaxy. The dust mass calculated based on the above dust temperature and emissivity index assumption is $M_{\mathrm{dust}} = (2.0 \pm 0.4) \times 10^8\,M_\odot$. We adopt a dust absorption coefficient of $\kappa_d(\lambda) \sim \lambda^{-\beta}$ and $\kappa_d(125\,\mu\mathrm{m}) = 18.75$ cm^2 g^{-1} (Hildebrand 1983) in the calculation. If a higher dust temperature of 60 K is adopted (i.e., the highest temperature seen among the (sub)mm-detected $z \sim 6$ quasars, Leipski et al. 2013), the FIR luminosity and SFR increase by a factor of 1.7,

and the dust mass will decrease by a factor of 1.8. If we adopt the lowest dust temperature of 40 K, found by Leipski et al. (2013), the FIR and SFR with decrease by a factor of 1.5, and the dust mass increases by a factor of 1.6 (Table 1).

The VLA *Ka-* and *S*-band observations measure the rest-frame 234 and 22 GHz continuum emission, respectively. The corresponding continuum luminosities are $\nu L_{\nu,234\,\mathrm{GHz}} = (5.8 \pm 1.7) \times 10^8\,L_\odot$ and $\nu L_{\nu,22\,\mathrm{GHz}} = (3.9 \pm 0.1) \times 10^8\,L_\odot$. We calculate the radio-loudness of this object, adopting the definition of $R = f_{\nu,5\,\mathrm{GHz}}/f_{\nu,4400\,\text{Å}}$ (Kellermann et al. 1989). The rest-frame 4400 Å flux density ($f_{\nu,4400\,\text{Å}}$) is interpolated using the scaled Richards et al. (2006) optically luminous quasar template (Figure 1), and the rest-frame 5 GHz flux density ($f_{\nu,5\,\mathrm{GHz}}$) is extrapolated from 22 GHz data assuming a power-law radio continuum of $f_\nu \propto \nu^\alpha$. This constrains the radio-loudness to be $R = 0.9$ for a steep spectrum of $\alpha = -0.9$, or $R = 0.2$ for a flat spectrum of $\alpha = -0.06$ (see below for the discussion of spectral index), indicating that this object is radio-quiet. However, the 234 and 22 GHz luminosities are more than an order of magnitude higher than the thermal bremsstrahlung or nonthermal synchrotron continuum expected from star-forming activities (e.g., Condon 1992; Yun et al. 2000; Yun & Carilli 2002; Zakamska et al. 2016). For instance, the thermal bremsstrahlung or nonthermal synchrotron continuum estimated with an SFR of 850 $M_\odot$ yr^{-1} using the formulae in Yun & Carilli (2002), contributes <5% of the detected continuum emission at both frequencies. Additionally, the thermal dust emission has only a minor contribution of 12%–21% to the 234 GHz flux density, based on the graybody models with $T_{\mathrm{dust}} = 60$–40 K described above. Thus, the continuum emission in J0100+2802 at frequencies of 234 GHz and lower is dominated by the radio activity of the central AGN.

In Figure 1, we adopt the graybody model with $T_{\mathrm{dust}} = 47$ K to remove the dust continuum at 234 GHz and fit a power law ($f_\nu \sim \nu^\alpha$) to the remaining 234 GHz flux density and the 22 GHz data. This estimates the 234–22 GHz two-point spectral index to be $\alpha_{22\,\mathrm{GHz}}^{234\,\mathrm{GHz}} = -0.90 \pm 0.15$. We also measure the spectral index within the *S*-band by averaging the data in every two 128 MHz spectral windows from the observed frequencies of 2.4–4 GHz. In contrast to the steep spectrum indicated by $\alpha_{22\,\mathrm{GHz}}^{234\,\mathrm{GHz}}$, the best-result fit to the seven data points in the *S*-band yields a flat spectrum with $\alpha_{22\,\mathrm{GHz}} = -0.06 \pm 0.22$. J0100+2802 provides a great example for studying the radio activity in the most optically luminous and radio-quiet nucleus at the earliest epoch. We will need further observations at multiple radio frequencies to check if the radio continuum is indeed flattened or inverse around 22 GHz. Additionally, milli-arcsecond resolution observations through Very Long Baseline interferometry are needed to measure the spatial extent of the radio source in this object and address if there are multiple components contributing to the detected radio continuum, as was widely discussed for the radio-quiet quasars at lower redshift (e.g., Ulvestad et al. 1999, 2005)
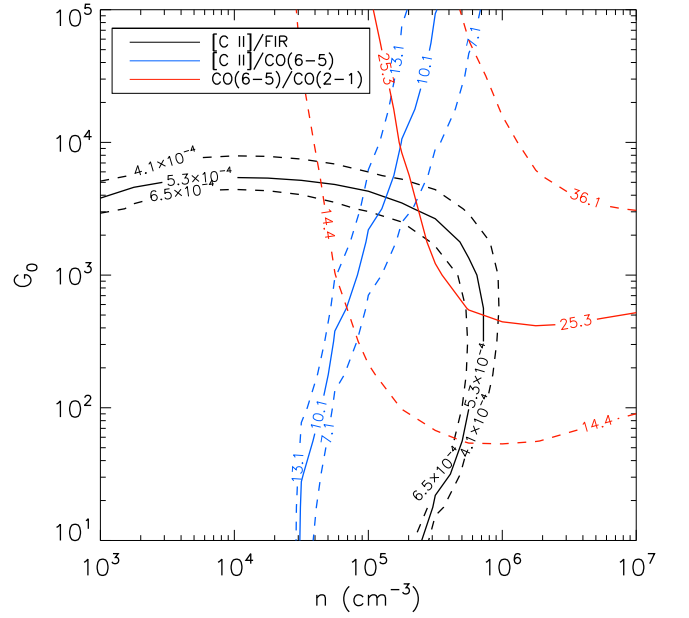
4.2. Luminosity Ratios and Gas Masses

Based on the FIR luminosity derived in the previous section, we constrain the [C II]-to-FIR luminosity ratio to be 0.0010 ± 0.0002. This is comparable to the values found in other [C II]-detected $z > 5.7$ quasars that have similar moderate FIR luminosities of $L_{\mathrm{FIR}} \lesssim 1 \times 10^{12}\,L_\odot$ to $\sim 4 \times 10^{12}\,L_\odot$, and

higher than that from the more FIR luminous objects ($L_{FIR} \geqslant 5 \times 10^{12} L_\odot$, Wang et al. 2013), i.e., following the trend of decreasing FIR luminosity with increasing [C II]-to-FIR luminosity ratios defined by the high-redshift quasars and starburst galaxies (Maiolino et al. 2009; Riechers et al. 2013; De Breuck et al. 2014; Gullberg et al. 2015; Muñoz & Oh 2015; Willott et al. 2015; Narayanan & Krumholz 2016; Venemans et al. 2016). The SFR estimated with the [C II] luminosity is 560 $M_\odot$ yr^{-1}, adopting the SFR-[C II] luminosity relation for high-redshift galaxies in De Looze et al. (2014). This is consistent with the SFR estimates based on the dust continuum.

The CO observations measure a CO (6-5)-to-(2-1) line flux ratio of 8.4 ± 3.6 and a line luminosity ratio of $L'_{CO(6-5)}/L'_{CO(2-1)} = 0.94 \pm 0.40$. This is consistent with the ratios found in other CO-detected $z > 5.7$ quasars within the errors (Wang et al. 2011; Stefan et al. 2015), suggesting that the detected CO emission is likely from a highly excited molecular gas component peaked at $J = 6$ or higher (Riechers et al. 2009; Gallerani et al. 2014; Stefan et al. 2015). If we assume that the low-J CO transitions are thermalized, i.e., $L'_{CO(1-0)} = L'_{CO(2-1)}$ (e.g., Carilli & Walter 2013), and adopt a luminosity-to-mass conversion factor of $\alpha_{CO} = 0.8\ M_\odot$ /K km s^{-1} pc^2 from the local ultraluminous infrared galaxies (Downes & Solomon 1998), the detected CO(2-1) line flux yields a molecular gas mass of $M_{mol} = (1.0 \pm 0.3) \times 10^{10}\ M_\odot$. However, the total molecular gas mass in the quasar host could be larger considering that some of the CO (2-1) line flux from the low surface brightness region and the line wings might be missing due to the poor S/N of the observation.

We compare the luminosity ratios of the FIR continuum, [C II], and CO lines from J0100+2802 to the models of the photodissociation region (PDR[13]; Kaufman et al. 1999, 2006; Pound & Wolfire 2008) in Figure 3 to investigate the gas density n and the incident far-ultraviolet radiation field G_0 (in units of the Habing Field, 1.6×10^{-3} ergs cm^{-2} s^{-1}) of the ISM in the quasar host galaxy. As a one-side illuminated slab geometry was adopted in the model, we here divide the optically thin FIR[14] and [C II] line emission by a factor of 2 to match the condition in the model. We also multiply $L_{[C II]}$ by a factor of 0.7 to estimate and exclude the [C II] emission from the diffuse region (Stacey et al. 1991; Colbert et al. 1999). According to Figure 3, the overlap region of the three luminosity ratios suggests a G_0 of a few thousand and $n \gtrsim 1 \times 10^5$ cm^{-3}. These are only preliminary constraints on the physical condition of the star-forming region in the host galaxy of J0100+2802. There are still large uncertainties in the calculation of FIR luminosity. The fractions of [C II] and CO emission from the PDR region are also not well-determined. A larger FIR luminosity with a higher T_{dust} will result in a higher G_0, and any contribution from the X-ray dominated regions (XDR) to the detected CO (6-5) line emission (e.g., Gallerani et al. 2014) will result in a higher $L_{[C II]}/L_{CO(6-5)}$ and a lower $L_{CO(6-5)}/L_{CO(2-1)}$ from the PDR region and move the best-fit gas density to $n < 10^5$ cm^{-3}.

We estimate the atomic gas mass within the PDR region from the [C II] line luminosity using Equation (1) in Hailey-Dunsheath et al. (2010), adopting the best-fit parameters

---

[13] The line and FIR ratio models are taken from the Photo Dissociation Region Toolbox (http://dustem.astro.umd.edu/pdrt/).

[14] The FIR luminosity is re-calculated in the range of 30–1000 μm to match the definition in the models.

Figure 3. Luminosity ratios of $L_{[C II]}/L_{FIR}$ (black), $L_{[C II]}/L_{CO(6-5)}$ (blue), and $L_{CO(6-5)}/L_{CO(2-1)}$ (red) compared to the PDR models of Kaufman et al. (1999) in different conditions of radiation field G_0 and gas density n. Luminosities are all in units of $L_\odot$. The dashed contours denote the $\pm 1\sigma$ error bars from the observing uncertainties. We adopt the optically thin graybody model with $T_{dust} = 47$ K and $\beta = 1.6$ to calculate L_{FIR}. The L_{FIR} here is integrated in the wavelength range of 30–1000 μm to match the FIR definition in the model. We also assume that 70% of the detected [C II] line emission is from the PDR region. Thus the $L_{[C II]}/L_{FIR}$ value in the plot is lower than the value of 0.001 quoted in Section 4.1. We also divide $L_{[C II]}$ and L_{FIR} by a factor of 2 to match the one-sided illuminated geometry in the model.

indicated in Figure 3 (i.e., $G_0 \sim 4000$, $n \sim 10^{5.1}$ cm^{-3}, and a corresponding PDR surface temperature of $T \sim 550$ K, Kaufman et al. 1999), a C$^+$ abundance of 1.4×10^{-4}, and a critical density of $n_{crit} = 2.7 \times 10^3$ cm^{-3}. The derived atomic gas mass in the PDR region is $M_{atomic,PDR} \sim 3 \times 10^9\ M_\odot$, which is about 30% of the molecular gas mass estimated with the CO (2-1) line. The mass ratio associated with the detected CO, [C II], and FIR dust emission is $(M_{mol} + M_{atomic,PDR})/M_{dust} \sim 65$. This is comparable to the mass ratios of other CO-detected quasars and dusty starburst galaxies at high-z (Michalowski et al. 2010; Wang et al. 2010; Riechers et al. 2013).

4.3. Constraint on Host Galaxy Dynamical Mass

Among the quasars known at $z > 6$, J0100+2802 has the most massive SMBH, with a mass of $(1.24 \pm 0.19) \times 10^{10}\ M_\odot$ (De Rosa et al. 2011; Wu et al. 2015). We use the [C II] line width (FWHM$_{[C II]}$) to present a preliminary estimate of the host galaxy mass for this object. We assume that the line is from a rotating gas disk and the circular velocity can be estimated as $v_{cir} = 0.75$FWHM$_{[C II]}/\sin(i)$, where i is the inclination angle between the rotation axis of the disk and the line of sight. The [C II] line emission from J0100+2802 is unresolved in our PdBI observation at 2$''$ resolution. According to the recent [C II] observations of other $z \sim 6$ quasars at sub-arcsecond resolution, the typical FWHM major axis sizes of the [C II] emission are about $2 \sim 4$ kpc (Wang et al. 2013; Willott et al. 2013, 2015; Venemans et al. 2016). Thus, we here estimate the FWHM [C II] source size for J0100+2802 to be 3 ± 1 kpc (see also Willott et al. 2015; Venemans et al. 2016) and set the diameter of the gas disk D as $1.5 \times$ the FWHM [C II]
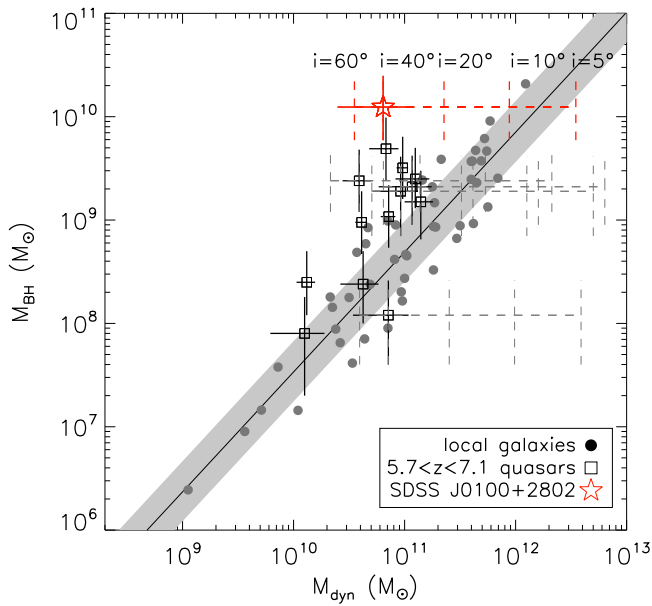
Figure 4. M_{BH} vs. M_{dyn} of the [C II]-detected $z > 5.7$ quasars. The M_{dyn} for $z > 5.7$ quasars are estimated based on [C II] observations, except for one object, SDSS J114816.64+525150.3 at $z = 6.42$, in which the [C II]-emitting gas at >1.5 kpc scale is turbulent and the CO size is adopted (Riechers et al. 2009; Wang et al. 2013; Willott et al. 2013, 2015; Cicone et al. 2015; Venemans et al. 2016). The red star shows J0100+2802 in this work. For objects that do not have an inclination angle estimated with the resolved [C II] image, we show M_{dyn} calculated with different inclination angles (dashed lines). The solid line and the gray region show the local relationship with ± 0.3 dex intrinsic scatter. The gray circles are the sample of local galaxies (Kormendy & Ho 2013).

source size, i.e., $D = 4.5 \pm 1.5$ kpc. The host galaxy dynamical mass is then $M_{dyn}(M_\odot) = 1.16 \times 10^5 \, v_{cir}^2 D = [2.6(D/4.5 \text{ kpc}) \pm 1.6] \times 10^{10}/\sin^2(i) M_\odot$. The error includes the uncertainties from both the line width and the assumed disk size.

We plot M_{BH} versus M_{dyn} for J0100+2802 and other $z > 5.7$ quasars in Figure 4 (Wang et al. 2013; Willott et al. 2013, 2015; Bañados et al. 2015; Venemans et al. 2016), comparing to the SMBH-to-bulge mass relation of local galaxies from Kormendy & Ho (2013), i.e., $M_{BH}/(10^9 \, M_\odot) = 0.49(M_{bulge}/10^{11} \, M_\odot)^{1.16}$. For J0100+2802 as well as other $z > 5.7$ quasars that have SMBH mass measurements based on the quasar Mg II line emission (De Rosa et al. 2011, 2014; Willott et al. 2013, 2015), we follow Willott et al. (2015) and add a 0.3 dex uncertainty to the error bar of the SMBH mass to account for the scatter of the calibration (Shen et al. 2008). For the sample from Wang et al. (2013), which does not have SMBH mass measurements, we adopt the relationship between the 1450 Å luminosity and the quasar bolometric luminosity from Venemans et al. (2016), and calculate the Eddington luminosities and SMBH masses assuming a typical Eddington ratio and a scatter of $\log(L_{bol}/L_{Edd}) = -0.3 \pm 0.3$ from De Rosa et al. (2011). The M_{dyn} for most of the $z > 5.7$ quasars are estimated based on [C II] observations (Wang et al. 2013; Willott et al. 2013, 2015; Bañados et al. 2015; Venemans et al. 2016). The only exception is the $z = 6.42$ quasar SDSS J114816.64+525150.3, in which the [C II]-emitting gas at >1.5 kpc scale is turbulent (Cicone et al. 2015) and the CO size is used (Riechers et al. 2009; Stefan et al. 2015) in the M_{dyn} calculation. According to Figure 4, for any inclination angle of

$i \geqslant 10°$, J0100+2802 is above the local $M_{BH}-M_{bulge}$ relation and the ± 0.3 dex area of the intrinsic scatter (i.e., the gray area in Figure 3). As was discussed in Willott et al. (2015), most of the $z \sim 6$ quasars with SMBH masses on the order of $10^8 \, M_\odot$ are close to the trend of local galaxies, while the more luminous and massive objects tend to be above this trend (see also Venemans et al. 2016). This suggests that the SMBH grows faster than the quasar host galaxies in these most massive systems at the earliest epoch, unless all these $M_{BH} > 10^9 \, M_\odot$ quasars are close to face-on. However, as there is no resolved image for J0100+2802 yet, we do not rule out the possibilities that the gas is unvirialized and the [C II] line width cannot probe the disk circular velocity.

5. SUMMARY

We detected [C II], CO, and (sub)mm and radio continuum emission in the host galaxy of the quasar J0100+2802, which hosts the most massive SMBH known at $z \geqslant 6$. The detections probe the properties of the young quasar host at an early evolutionary stage: the (sub)mm continuum indicates moderate FIR emission and constrains the SFR to be $\leqslant 850 \, M_\odot \, \text{yr}^{-1}$. The CO and [C II] lines estimate the gas mass and gas-to-dust mass ratio that are within the range of other millimeter-detected quasars at $z \sim 6$. The [C II]-to-FIR luminosity ratio J0100 +2802 is higher than that of the most FIR luminous quasars at $z > 5.7$, i.e., following the trend of increasing $L_{[C II]}/L_{FIR}$ with decreasing L_{FIR} found for high-z quasars and star-forming systems. The quasar Mg II line emission detected in previous near-infrared spectroscopic observations (Wu et al. 2015) is blueshifted by about 1000 km s^{-1} compared to the host galaxy redshift measured by the [C II] and CO lines. The host dynamical mass estimated with the [C II] line width suggests that the SMBH is likely to be overmassive, compared to the local relation, though further constraints on the gas kinematics and disk inclination angle are still required.

Facilities: IRAM (PdBI), VLA, JCMT (SCUBA-2).

REFERENCES

Bañados, E., Decarli, R., Walter, F., et al. 2015, ApJL, 805, 8
Bañados, E., Venemans, B. P., Morganson, E., et al. 2014, AJ, 148, 14
Beelen, A., Cox, P., Bertoldi, F., et al. 2006, ApJ, 642, 694
Bertoldi, F., Cox, P., Neri, R., et al. 2003, A&A, 409, L47
Carilli, C. L., Neri, R., Wang, R., et al. 2007, ApJL, 666, L9
Carilli, C. L., & Walter, F. 2013, ARA&A, 51, 105
Chapin, E. L., Berry, D. S., Gibb, A. G., et al. 2013, MNRAS, 430, 2545
Cicone, C., Maiolino, R., Gallerani, S., et al. 2015, A&A, 574, 14
Colbert, J. W., et al. 1999, ApJ, 511, 721
Condon, J. J. 1992, ARA&A, 30, 575
De Breuck, C., Williams, R. J., Swinbank, M., et al. 2014, A&A, 565, 59
De Looze, I., Cormier, D., Lebouteiller, V., et al. 2014, A&A, 568, 62
De Rosa, G., Decarli, R., Walter, F., et al. 2011, ApJ, 739, 56
De Rosa, G., Venemans, B. P., Decarli, R., et al. 2014, ApJ, 790, 145
Downes, D., & Solomon, P. M. 1998, ApJ, 507, 615
Elvis, M., Wilkes, B. J., McDowell, J. C., et al. 1994, ApJS, 95, 1
Fan, X., Strauss, M. A., Richards, G. T., et al. 2006, AJ, 131, 1203
Gallerani, S., Ferrara, A., Neri, R., & Maiolino, R. 2014, MNRAS, 445, 2848
Guilloteau, S., & Lucas, R. 2000, ASPC, 217, 299
Gullberg, B., De Breuck, C., Vieira, J. D., et al. 2015, MNRAS, 449, 2883
Hailey-Dunsheath, S., Nikola, T., Stacey, G. J., et al. 2010, ApJL, 714, L162
Hildebrand, R. H. 1983, QJRAS, 24, 267
Holland, W. S., Bintley, D., Chapin, E. L., et al. 2013, MNRAS, 430, 2513
Jiang, L., McGreer, I. D., Fan, X., et al. 2015, AJ, 149, 188
Kaufman, M. J., Wolfire, M. G., & Hollenbach, D. J. 2006, ApJ, 644, 283
Kaufman, M. J., Wolfire, M. G., Hollenbach, D. J., & Luhman, M. L. 1999, ApJ, 527, 795
Kellermann, K. I., Sramek, R., Schmidt, M., Shaffer, D. B., & Green, R. 1989, AJ, 98, 1195
Kennicutt, R. C., Jr. 1998, ARA&A, 36, 189
Kormendy, J., & Ho, L. C. 2013, ARA&A, 51, 511

Leipski, C., Meisenheimer, K., Walter, F., et al. 2013, ApJL, 772, 103
Maiolino, R., Caselli, P., Nagao, T., et al. 2009, A&A, 500, L1
Matsuoka, Y., Onoue, M., Kashikawa, N., et al. 2016, ApJ, submitted (arXiv:1603.02281)
McConnell, N. J., Ma, C.-P., Gebhardt, K., et al. 2011, Natur, 480, 215
Michalowski, M. J., Watson, D., & Hjorth, J. 2010, ApJ, 712, 942
Muñoz, J. A., & Oh, S. P. 2015, MNRAS, submitted (arXiv:1510.00397)
Narayanan, D., & Krumholz, M. 2016, MNRAS, submitted (arXiv:1601.05803)
Omont, A., Willott, C. J., Beelen, A., et al. 2013, A&A, 552, A43
Petric, A. O., Carilli, C. L., Bertoldi, F., et al. 2003, AJ, 126, 15
Pound, M. W., & Wolfire, M. G. 2008, ASPC, 394, 654
Priddey, R. S., Isaak, K. G., McMahon, R. G., et al. 2003, MNRAS, 339, 1183
Richards, G. T., Lacy, M., Storrie-Lombardi, L. J., et al. 2006, ApJS, 166, 470
Richards, G. T., Vanden Berk, D. E., Reichard, T. A., et al. 2002, AJ, 124, 1
Riechers, D. A., Bradford, C. M., Clements, D. L., et al. 2013, Natur, 496, 329
Riechers, D. A., Walter, F., Bertoldi, F., et al. 2009, ApJ, 703, 1338
Robson, I., Priddey, R. S., Isaak, K. G., et al. 2004, MNRAS, 351, L29
Shen, Y., Greene, J. E., Strauss, M. A., Richards, G. T., & Schneider, D. P. 2008, ApJ, 680, 169
Solomon, P. M., & Vanden Bout, P. A. 2005, ARA&A, 43, 677
Spergel, D. N., Bean, R., Doré, O., et al. 2007, ApJS, 170, 377
Stacey, G. J., Geis, N., Genzel, R., et al. 1991, ApJ, 373, 423
Stefan, I. I., Carilli, C. L., Wagg, J., et al. 2015, MNRAS, 451, 1713
Thomas, J., Ma, Ch.-P., McConnell, N. J., et al. 2016, Natur, 532, 340
Ulvestad, J. S., Antonucci, R. R. J., & Barvainis, R. 2005, ApJ, 621, 123
Ulvestad, J. S., Wrobel, J. M., & Carilli, C. L. 1999, ApJ, 516, 127
Venemans, B. P., Bañados, E., & Decarli, R. 2015, ApJL, 801, L11
Venemans, B. P., Walter, F., Zschaechner, L., et al. 2016, ApJ, 816, 37
Walter, F., Carilli, C. L., Bertoldi, F., et al. 2004, ApJL, 615, L17
Wang, R., Carilli, C., Neri, R., et al. 2010, ApJ, 714, 699
Wang, R., Wagg, J., Carilli, C., et al. 2011, ApJL, 739, L34
Wang, R., Wagg, J., Carilli, C., et al. 2013, ApJ, 773, 44
Willott, C. J., Bergeron, J., & Omont, A. 2015, ApJ, 801, 123
Willott, C. J., Delorme, P., Reylé, C., et al. 2010, AJ, 139, 906
Willott, C. J., Omont, A., & Bergeron, J. 2013, ApJ, 770, 13
Wu, X.-B., Wang, F., Fan, X., et al. 2015, Natur, 518, 512
Yun, M. S., & Carilli, C. L. 2002, ApJ, 568, 88
Yun, M. S., Carilli, C. L., Kawabe, R., et al. 2000, ApJ, 528, 171
Zakamska, N. L., Lampayan, K., Petric, A., et al. 2016, MNRAS, 455, 4191